Magic angle spinning nuclear magnetic resonance studies of molecular motion in cross-linked polyethylene

G. Scholtyssek, J. Sohma* and H. G. Zachmann†
Institut für Technische und Makromolekulare Chemie, University of Hamburg, Bundestrasse 45, D-2000 Hamburg 13, FRG
(Received 2 January 1990; accepted 21 May 1990)

Magic angle spinning nuclear magnetic resonance spectroscopic investigations were performed on solid state high density polyethylene (HDPE) and low density polyethylene (LDPE) crosslinked by γ-irradiation using doses up to 40 Mrad. The free induction decay was measured at various spinning frequencies in order to obtain information on the influence of crosslinks and branches on molecular mobility in the amorphous regions of the semicrystalline material. The anisotropy of motion caused by crosslinks and entanglements is characterized by the anisotropy parameter, a, and the correlation time of anisotropy fluctuations τ_{ca}. It was found that in HDPE the values of a are larger and those of τ_{ca} are smaller than in LDPE. In HDPE crosslinking leads to a shift of the spectrum of a to larger values whereas in LDPE no change is observed upon irradiation. However, if the material is molten, upon irradiation the molecular mobility is markedly decreased in both HDPE and LDPE. The results are discussed comparing densities of crosslinks and entanglements.

(Keywords: nuclear magnetic resonance; magic angle spinning; polyethylene; irradiation; molecular motion)

INTRODUCTION

It is well known that crosslinks restrict the motion of the molecules in a polymer. The same is true for chain entanglements. For example, in the vicinity of either a crosslink or an entanglement in an amorphous polymer, the molecular motion cannot be assumed to be isotropic.

It has been well established that nuclear magnetic resonance (n.m.r.) is a powerful tool for investigating the molecular mobility in polymers. Broad line n.m.r. was used to study the effect of crosslinks on molecular mobility in polymers more than two decades ago[1,2]. Pulse n.m.r. technique was introduced later on[3–5]. Generally, in n.m.r. investigations molecular mobility is characterized by two relaxation times, the spin-lattice relaxation time (T_1) and the spin–spin relaxation time (T_2). They are both influenced by the spectrum of correlation times, $f(\tau_c)$, which describes the molecular mobility quantitatively.

Recently, the magic angle spinning (MAS) technique was successfully applied to pulse proton n.m.r. measurements of chain mobility[6–9]. In this technique the sample is rotating around an axis including the 'magic angle' of 54°44′ with the static magnetic field. It was found that the n.m.r. line-shape is strongly affected by the rotational frequency $\omega_r = 2\pi\nu_r$. This means that n.m.r. measurements at variable ω_r provide a new window on the time scale, which is very important for studies of molecular mobility. The new parameter ω_r could be used to collect information in a time domain, which has not been detected by other time scales used in conventional n.m.r. measurements. In addition, novel information on both the anisotropy of the molecular motion and the time scale governing the change of this anisotropy is obtained.

An interesting problem is the influence of chemical crosslinks on the mobility of polymer chains. Corresponding n.m.r. studies on irradiated polyethylene were performed by Charlesby and co-workers[3–5]. However, magic angle spinning was not applied in these studies.

In the present paper, a brief account is given of the theory describing the free induction decay (f.i.d.) as a function of both ω_r and correlation times. Experimental results obtained on the influence of the magic angle spinning frequency ω_r on the n.m.r. signal of irradiated and non-irradiated polyethylene will be discussed on the basis of this theory and new results concerning the influence of crosslinks on the molecular mobility in the amorphous regions of polyethylene will be presented.

EXPERIMENTAL

Samples

Two kinds of polyethylene were investigated, a high density polyethylene (HDPE) made by Ube Kosan Co. in Japan (UBE C 400) and a low density polyethylene (LDPE) made by Showa Denko Co. in Japan (SHOLEX 6050). The molecular weights determined by viscometry were 9.3×10^4 for HDPE and 4.4×10^4 for LDPE. The crystallinities determined by density measurements were 73% for HDPE and 50% for LDPE.

The two polymers were γ-irradiated at various doses up to 40 Mrad by using a ^{60}Co source (in the Takasaki Research Laboratory of the Japan Atomic Energy

* Present address: Faculty of Science, Kanagawa University, 2946 Tsuchiya, Hiratsuka 259-12, Japan
† To whom correspondence should be addressed

0032-3861/91/061031-13

Table 1 Average crosslink densities of the polyethylene samples

Irradiation dose (Mrad)	Crosslink density in LDPE (crosslinks cm^{-3})	Crosslink density in HDPE (crosslinks cm^{-3})
0	0	0
10	1.00×10^{19}	0.82×10^{19}
20	2.00×10^{19}	1.64×10^{19}
30	3.00×10^{19}	2.46×10^{19}
40	4.00×10^{19}	3.28×10^{19}

Research Institute). The average crosslink densities (crosslinks per cm^3) produced by the irradiation were determined by the Charlesby–Pinner method[10] from the observed sol fractions after the irradiation and are shown in *Table 1*.

Method

The measurements were performed on the n.m.r. spectrometer CXP-100 from Bruker using a high power probehead. The temperature was controlled by streaming hot air. Magic angle spinning was performed by means of a self-constructed turbine described earlier[8]. The spinning frequencies ω_r were determined acoustically using a microphone to record the acoustic waves and measuring the frequency on an oscilloscope. In cases where spinning side bands were observed on the n.m.r. line, ω_r was also determined from the position of these bands. The magic angle was adjusted by finding the position of the turbine at which the width of the n.m.r. line of a suitable material, e.g. polybutadiene, was at a minimum.

The quantity determined in our experiments was the f.i.d. of the transversal magnetization $M_\perp(t)$. A 90° pulse was applied and the resulting decrease of $M_\perp$ was measured. The measurements above the melting point were performed using Meiboom–Gill pulse sequences because, in the melt, the relaxation time T_2 is comparatively large and the influence of the inhomogeneity of the magnetic field is no longer negligible. The waiting time between the pulses was 2 ms. It was proved that no spin locking occurred when using this waiting time.

THEORY

Anisotropic motion and the effect of MAS

In a rigid system of CH_2 groups, a broad n.m.r. line and a short transversal relaxation time T_2 are observed, due to dipolar interaction of the H-atoms. If a rapid isotropic motion of the chain molecules occurs, the local magnetic field experienced by each H-atom fluctuates about the value zero (see *Figure 1a*) and is thus averaged to zero. Therefore, the n.m.r. line becomes very narrow and the transversal relaxation time T_2 is comparatively large. The condition for this motional narrowing is given by $\tau_c \ll T_2$, where τ_c is the correlation time characterizing the rapid motion.

In the case of an anisotropic motion occurring, for example if the ends of a molecular chain are fixed in space, the fluctuation of the local magnetic field, H_{loc}, occurs about a value which is different from zero and therefore the average value of the local field is not zero, i.e. $\langle H_{loc} \rangle \neq 0$ (*Figure 1b*). Consequently, the n.m.r. line is broadened and T_2 is decreased if compared to the case of quick isotropic motion.

Of special interest is the case indicated in *Figure 1c*, in which $\langle H_{loc} \rangle$ itself fluctuates about the value zero with the correlation time τ_{ca}, which is considerably larger than τ_c. This occurs, for example, in a melt of entangled chain molecules. The motion of the CH_2 group, designated by A in *Figure 2*, is anisotropic because the group is part of a chain of which the ends are temporarily fixed by the entanglements 1 and 2. The residual local magnetic field has a value $\langle H_{loc} \rangle = H_1$ which is different from zero. This situation, however, does not last for infinite time. After some characteristic time, τ_{ca}, the restrictions in motion will be changed, for example because the CH_2 group has moved by reptation to position B in *Figure 2*. The chain to which the group belongs is now fixed at two other

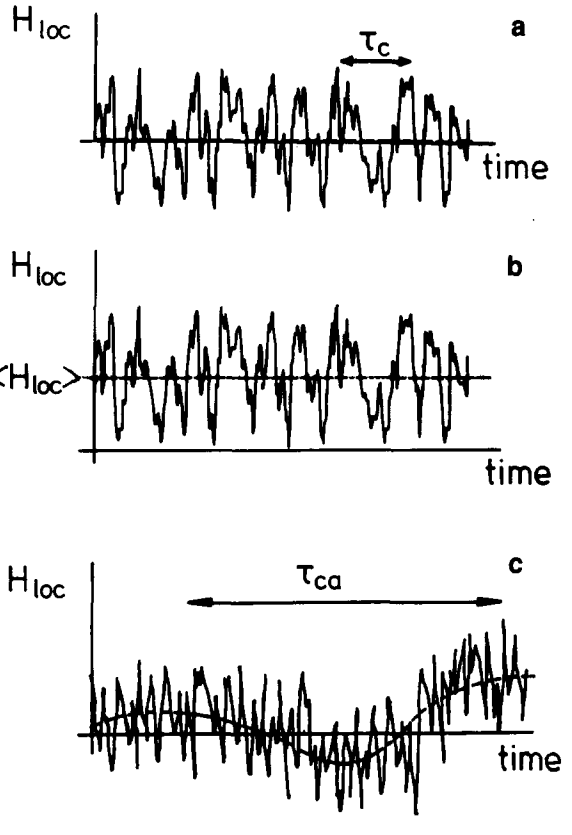

Figure 1 Change of the local magnetic field H_{loc} with time. (a) Isotropic motion; (b) anisotropic motion with locally fixed restrictions; (c) anisotropic motion with fluctuating restrictions

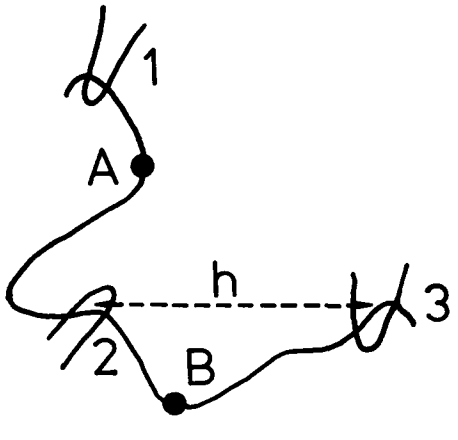

Figure 2 Schematic representation of the mobility restriction of a chain by entanglements

points, 2 and 3. As the vector from point 2 to point 3 has a different direction to the vector from point 1 to point 2, the residual local magnetic field has a value $\langle H_{loc}\rangle = H_2$ which is different from H_1.

As shown by Andrew and Jasinski[6], in the case of magic angle spinning the effective residual local field $\langle H_{loc}\rangle$ is zero, if, in addition to $\tau_c \ll T_2$, the rotation frequency ω_r fulfils the following two conditions:

$$\omega_r > 1/T_2 \tag{1}$$

$$\omega_r > 1/\tau_{ca} \tag{2}$$

Equations for the time decay of transversal magnetization

An exact equation for the time decay of transversal magnetization $M_\perp(t)$ has been derived by Spiess[11], Müller[12] and Scholtyssek[13]. The parameters determining this decay are as follows.

1 The frequency of magic angle spinning ω_r: technically accessible values of the spinning frequency range from 0 to 10 kHz.
2 The second moment of the n.m.r. spectrum in the case of rigid atoms and no magic angle spinning: $M_2 = \langle \Delta\omega^2 \rangle = (9/320\pi^2)\gamma^4\hbar^2\mu_0^2\Sigma r_{ik}^{-6}$. A typical value of M_2 is $10^{10}\ s^{-2}$.
3 The correlation time of the rapid motion of the atoms τ_c: Above glass transition temperature, this correlation time is of the order of magnitude of 10^{-10} to 10^{-7} s.
4 The correlation time τ_{ca} characterizing the change of anisotropy of parts of chains as described in *Figure 1*.
5 The anisotropy factor a ranging from zero (isotropic motion) to 1 (maximum anisotropy in case of the completely elongated chains). The exact definition of a can be found elsewhere[6,12,13].

The general expression for $M_\perp(t)$ is quite complicated. Some simplification is obtained for systems above glass transition temperature, where τ_c is comparatively small. Here the following relations hold:

$$(1-a)M_2\tau_c^2 \ll 1 \tag{3}$$

and

$$\omega_r\tau_c \ll 1 \tag{4}$$

Under these conditions one obtains

$$\begin{aligned} M_\perp(t) = \exp\Bigg\{ & -(1-a)M_2\tau_c t - aM_2\tau_{ca}^2 \\ & \times \Bigg\{ \frac{t}{\tau_{ca}} \left[\frac{2}{3}\frac{1}{1+\omega_r^2\tau_{ca}^2} + \frac{1}{3}\frac{1}{1+4\omega_r^2\tau_{ca}^2} \right] \\ & - \left[\frac{2}{3}\frac{1-\omega_r^2\tau_{ca}^2}{(1+\omega_r^2\tau_{ca}^2)^2} + \frac{1}{3}\frac{1-4\omega_r^2\tau_{ca}^2}{(1+4\omega_r^2\tau_{ca}^2)^2} \right] \\ & + e^{-t/\tau_{ca}} \left[\frac{2}{3}\frac{(1-\omega_r^2\tau_{ca}^2)\cos\omega_r t - 2\omega_r\tau_{ca}\sin\omega_r t}{(1+\omega_r^2\tau_{ca}^2)^2} \right. \\ & \left. + \frac{1}{3}\frac{(1-4\omega_r^2\tau_{ca}^2)\cos 2\omega_r t - 4\omega_r\tau_{ca}\sin 2\omega_r t}{(1+4\omega_r^2\tau_{ca}^2)^2} \right] \Bigg\} \Bigg\} \end{aligned} \tag{5}$$

For $\omega_r = 0$ this equation becomes:

$$M_\perp(t) = \exp\left\{ -(1-a)M_2\tau_c t - aM_2\tau_{ca}^2 \left(\frac{t}{\tau_{ca}} - 1 + e^{-t/\tau_{ca}} \right) \right\} \tag{6}$$

In the case of

$$aM_2\tau_{ca}^2 \ll 1 \tag{7}$$

corresponding to small anisotropy and/or fast fluctuations of anisotropy, one obtains from equation (6):

$$M_\perp(t) = \exp\{-[aM_2\tau_{ca} + (1-a)M_2\tau_c]t\} \tag{8}$$

Another limiting case is obtained if $\omega_r \gg 1/\tau_{ca}$. In the case of $aM_2\tau_{ca} \ll 1$, equation (5) then becomes:

$$M_\perp(t) = \exp\{-(1-a)M_2\tau_c t\} \tag{9}$$

Shape of the f.i.d. curves

The f.i.d. curves describe the time decay of the transversal magnetization as described by the equations given above. Considering the case of a sample which is not rotated ($\omega_r = 0$), if the condition of equation (7) is fulfilled, according to equation (8) an exponential decay with the following relaxation time is observed:

$$T_2 = 1/[M_2(a\tau_{ca} + (1-a)\tau_c)] \tag{10}$$

If the condition of equation (7) is not fulfilled, according to equation (6) the curve is Gaussian at low values of t and becomes more and more exponential with increasing time. Some examples of calculated curves are shown in *Figure 3*. In extreme cases the curve becomes completely Gaussian or completely exponential. However, for the following discussion it is important to state that the second derivative of $\ln M_\perp$ with respect to time is always negative. For this reason it is not possible to separate this curve into different exponential curves with different T_2 values. Therefore, if such a separation is possible, this always indicates that different values of a exist and/or a spectrum of τ_{ca}. Of course, this is only valid under the assumption that all protons are equivalent and contribute the same value of the second moment M_2 to the n.m.r. line.

In the investigations reported in this work, we separated the f.i.d. arising from the amorphous regions in a rapid decreasing Gaussian component and one or two more slowly decreasing Lorentzian curves (see equations (10) and (11)).

Upon magic angle spinning, according to equation (5) the following effects occur.

1 The monotonic decrease of $M_\perp$ with time becomes slower due to the factor in front of τ_{ca} in the second term of the first exponent in equation (5).
2 $M_\perp(t)$ oscillates due to the functions $\sin\omega_r t$ and $\cos\omega_r t$ in equation (5). If we consider $\ln M_\perp(t)$, the amplitude of the oscillation decays exponentially, the decay time being equal to τ_{ca}.

As an example, *Figure 4* shows some free induction decay curves in the case of MAS with the frequency $\nu_r = 2$ kHz.

The shape of the signal is changed if $\omega_r \gtrsim 1/\tau_{ca}$ and $\omega_r \gtrsim \sqrt{aM_2}$. In the case of $\omega_r \gg 1/\tau_{ca}$, according to equation (9), the decay becomes exponential and is characterized by the plateau relaxation time, T_{2p} given by:

$$T_{2p} = 1/M_2(1-a)\tau_c \tag{11}$$

By fitting the theoretical curves calculated by means of equation (5) to the experimental f.i.d. curves, one can determine τ_c, τ_{ca} and a. The detailed procedure is described in the section *Determination of the anisotropy parameters* a *and* τ_{ca}.

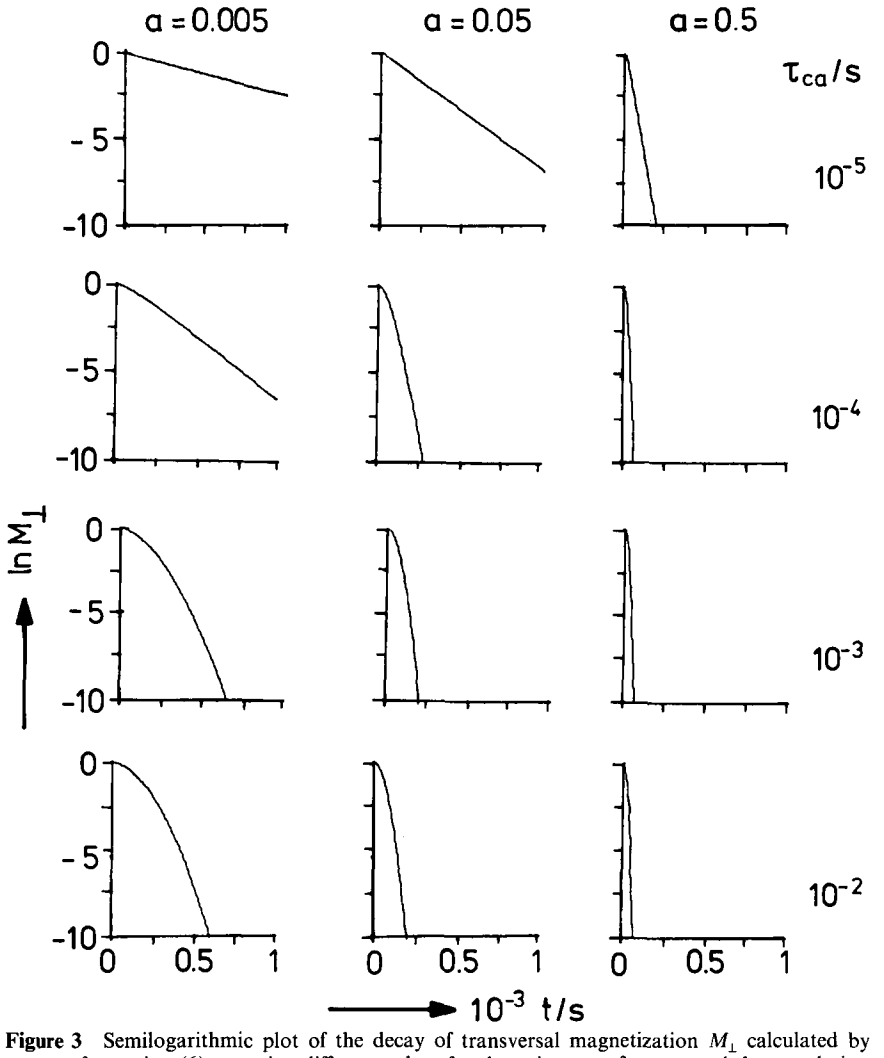

Figure 3 Semilogarithmic plot of the decay of transversal magnetization $M_\perp$ calculated by means of equation (6) assuming different values for the anisotropy factor a and the correlation time τ_{ca}, in the case of no rotation. ($\nu_r = 0$, $M_2 = 10^{10}\ s^{-2}$, $\tau_c = 2 \times 10^{-7}$ s)

The anisotropy of motion caused by fixing the ends of the chains at a certain distance h (see *Figure 2*) can also be characterized by the ratio h/h_0, h_0 being the end to end distance of the completely elongated chain[14–16]. If $h/h_0 = 1$, no segmental motion is possible. If $h/h_0 = 0$, the motion becomes isotropic. The relation between the average value $\langle h/h_0 \rangle$ and the increase of $1/T_2$ due to anisotropic motion has been calculated previously[13,14]. It is assumed that $T_2^{-1} = \Delta B\gamma/2$ where ΔB is the half width of the n.m.r. line. If this increase is designated by $1/T_{2a}$, it follows:

$$1/T_{2a} = 1/T_{2n} - 1/T_{2p} \qquad (12)$$

where T_{2n} is the relaxation time of the sample measured when no spinning occurs and T_{2p} is the plateau value obtained at sufficient high spinning frequency (see equation (11) and *Figure 13*).

RESULTS

Method of separation of the n.m.r. signal into different components

Generally, the free induction decay (f.i.d.) curve of polyethylene at room temperature consists of a rapidly decreasing and a slowly decreasing component. The rapidly decreasing component is attributed to the chains in the crystalline regions (and eventually to some taut amorphous chains) while the slowly decreasing component arises from the chains in the amorphous regions. Correspondingly, the n.m.r. absorption spectrum consists of a broad line, which is the Fourier transform of the rapidly decreasing component, and of a narrow line, which is the Fourier transform of the slowly decreasing component. For all measurements in this study, the contribution of the amorphous regions has been separated from the total spectrum using the method proposed by Klüver and Ruland[17] with some modifications. As in the method of Klüver and Ruland it is assumed that the crystals show an n.m.r. line with the shape of a Pake diagram (arising from the interaction of the protons in each CH_2 group) convoluted by a Gaussian curve (arising from the interaction of different CH_2 groups). However, in contrast to the method of Klüver and Ruland, it is assumed that the amorphous regions contribute not only exponential curves but also one Gaussian curve to the f.i.d. The Gaussian contribution accounts for the taut chains in the amorphous regions. By this method good agreement is obtained between the degree of crystallinity determined by n.m.r. and that obtained by density and X-ray measurements. The values that Klüver and Ruland obtained by n.m.r. were too large.

The contribution of the amorphous regions only is considered in the following. *Figure 5* shows the f.i.d. curve and the corresponding n.m.r. spectrum of non-irradiated

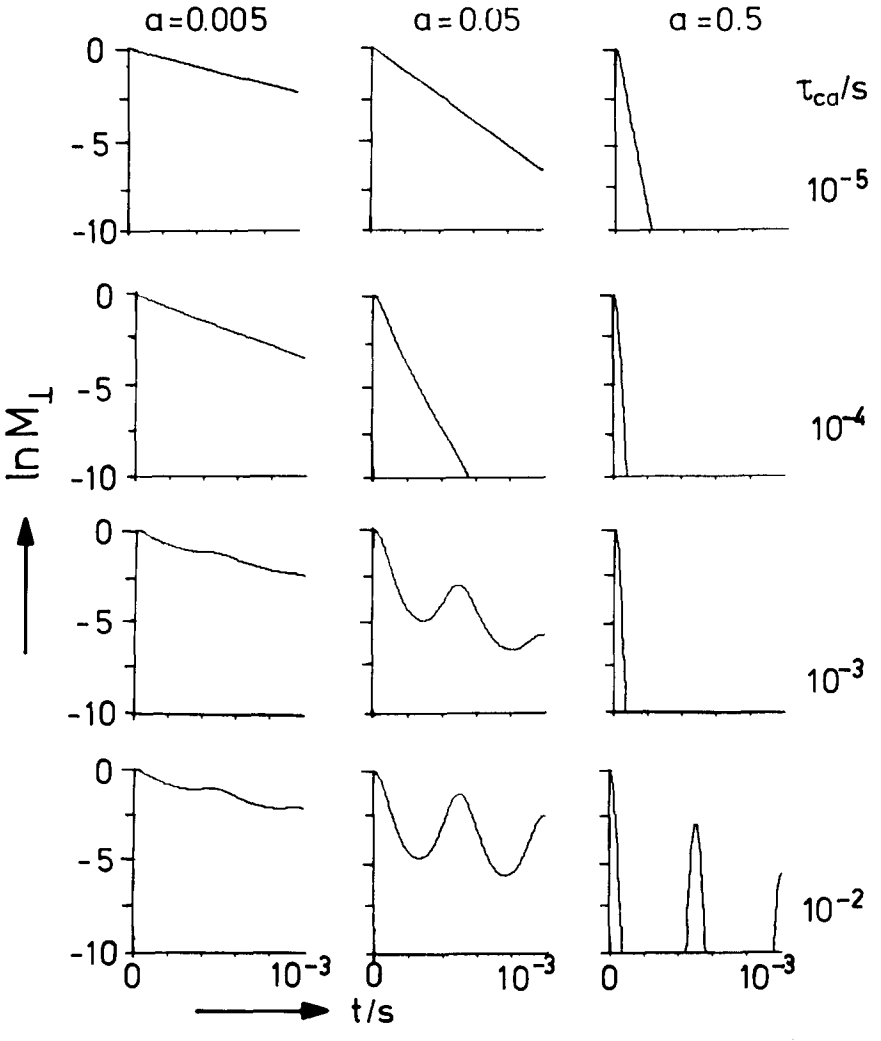

Figure 4 Semilogarithmic plot of the decay of transversal magnetization $M_\perp$ calculated by means of equation (5) assuming different values for the anisotropy factor a and the correlation time τ_{ca} in the case of MAS. ($\nu_r = 2$ kHz, $M_2 = 10^{10}\,s^{-2}$, $\tau_c = 2 \times 10^{-7}$ s)

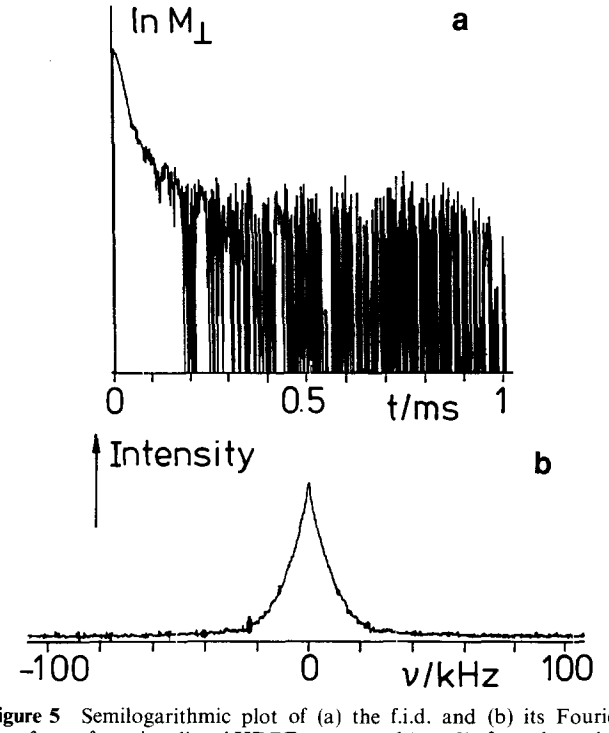

Figure 5 Semilogarithmic plot of (a) the f.i.d. and (b) its Fourier transform of non-irradiated HDPE not rotated ($\nu_r = 0$) after subtraction of the crystalline component

HDPE after the contribution of the crystalline regions has been subtracted as described above. Obviously, the f.i.d. curve is not exponential. The corresponding results obtained under magic angle spinning at a frequency of 6 kHz are represented in *Figure 6*. As a consequence of spinning, the intensity of the more rapid decreasing part of the f.i.d. curve is decreased. In addition, the f.i.d. trace becomes modulated and in the n.m.r. spectrum at least three pairs of spinning side bands appear. In *Figure 6a*, the f.i.d. trace is shown to consist of three components: a very rapidly relaxing Gaussian component (component 1); a slowly relaxing exponential component (component 2) and a slowly relaxing and modulated component (component 3). For further evaluation, these components are separated by using the following equation for the time decay of the transversal magnetization $M_\perp$:

$$M_\perp(t) = w_1 \exp(-t/T_2^{(1)})^2 + w_2 \exp(-t/T_2^{(2)}) + w_3 \exp(-t/T_2^{(3)}) \sum_n P_n \cos(n\omega_r t) \qquad (13)$$

This enables determination of the fractions w_1, w_2, w_3 and the decay times $T_2^{(1)}$, $T_2^{(2)}$, $T_2^{(3)}$ of the components 1, 2 and 3 respectively.

Relaxation behaviour of the solid sample

Figure 7 shows the rotation frequency dependence of

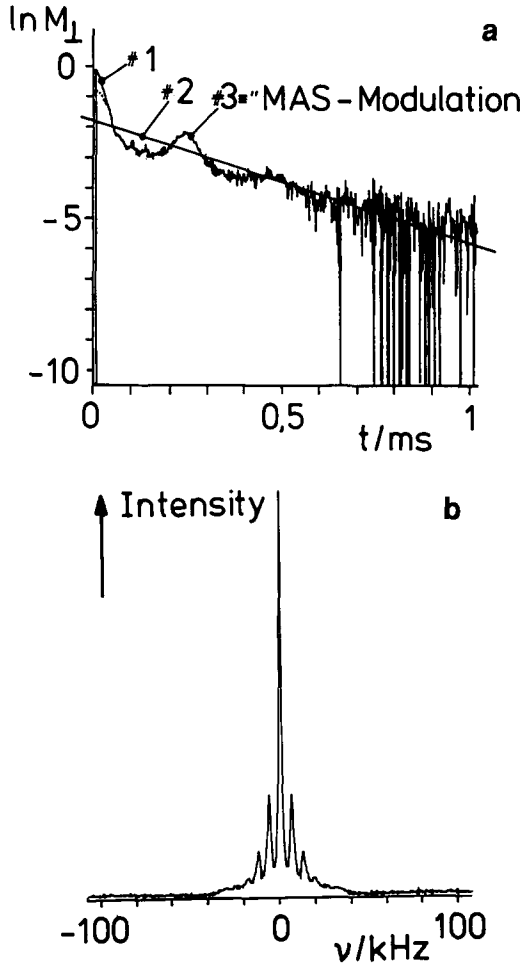

Figure 6 Semilogarithmic plot of (a) the FID and (b) its Fourier transform of non-irradiated HDPE under MAS ($\nu_r = 6$ kHz) after subtraction of the crystalline component

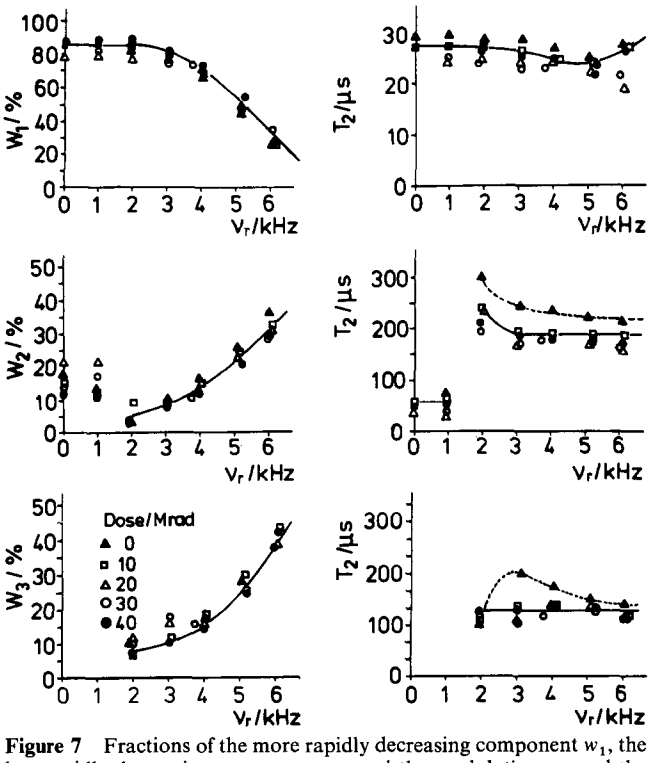

Figure 7 Fractions of the more rapidly decreasing component w_1, the less rapidly decreasing component w_2 and the modulation w_3 and the corresponding relaxation times T_2 of the f.i.d. curves from the amorphous regions of differently irradiated HDPE, as a function of rotation frequency ν_r. Irradiation dose: ▲, 0; □, 10; △, 20; ○, 30; ●, 40 Mrad

the fractions w_1, w_2, w_3 and of the decay times $T_2^{(1)}$, $T_2^{(2)}$ and $T_2^{(3)}$ of the three components of the n.m.r. signal from the amorphous regions of the HDPE samples at 25°C. For all samples, the fraction of component 1, which corresponds to the broad component of the spectrum, decreases with increasing rotational frequency ν_r while the fractions of the other components increase. This is the magic angle spinning effect. No remarkable difference between the non-irradiated HDPE and the irradiated HDPE was found. The decay times are only slightly affected by ν_r. The non-irradiated sample has longer relaxation times than the irradiated ones indicating differences in the correlation time spectrum (see *Discussion*).

A similar dependence of the w_i and the $T_2^{(i)}$ on ν_r was found for LDPE here. In this material, however, no difference between irradiated and non-irradiated samples was observed.

If the temperature of the sample is raised, all decay times increase while the difference between the f.i.d. curves of the irradiated sample and the non-irradiated sample remains as small as at room temperature. However, a significant effect of irradiation is observed above the melting point as shown in the following section.

Relaxation behaviour of the molten samples

Above the melting point the relaxation times are much larger than in the solid state. Therefore, the transversal relaxation curves were measured using Meiboom–Gill pulse sequences. *Figure 8* shows the relaxation curves of the non-irradiated and irradiated samples at 150°C at the various doses of irradiation. For further evaluation, each curve was decomposed into three components using the equation:

$$M_\perp(t) = w_1 \exp(-t/T_2^{(1)}) + w_2 \exp(-t/T_2^{(2)}) + w_3 \exp(-t/T_2^{(3)}) \quad (14)$$

The decomposition was achieved by fitting the curves using the least square method.

The results obtained for LDPE are shown in *Figure 9b* where the fractions w_i and the relaxation times $T_2^{(i)}$ are plotted as functions of the irradiation dose. The values of T_2 of component 1 decrease and the fraction of this component increases with increasing crosslink density. This result indicates a decrease in the mobility of the most slowly moving fraction in the sample while the amount of this fraction slightly increases. The T_2 values of the other two components also decrease with increasing doses of irradiation while the fractions of both components remain almost unchanged. This means that the hindrance caused by the crosslinks has most effect on the most mobile part of the chains.

The corresponding results obtained for HDPE are presented in *Figure 9a*. The T_2 value of component 1 decreases abruptly upon irradiation at a dose of 10 Mrad and stays nearly constant with increasing radiation dose. Similar abrupt changes are observed for the other components and for the fractions of the different components. Obviously, in contrast to the behaviour of LDPE, the largest effect comes from the first comparatively small dosage of irradiation of only 10 Mrad.

Relaxation behaviour after recrystallization from the melt

The completely molten samples were cooled down from 150°C to room temperature and kept at this

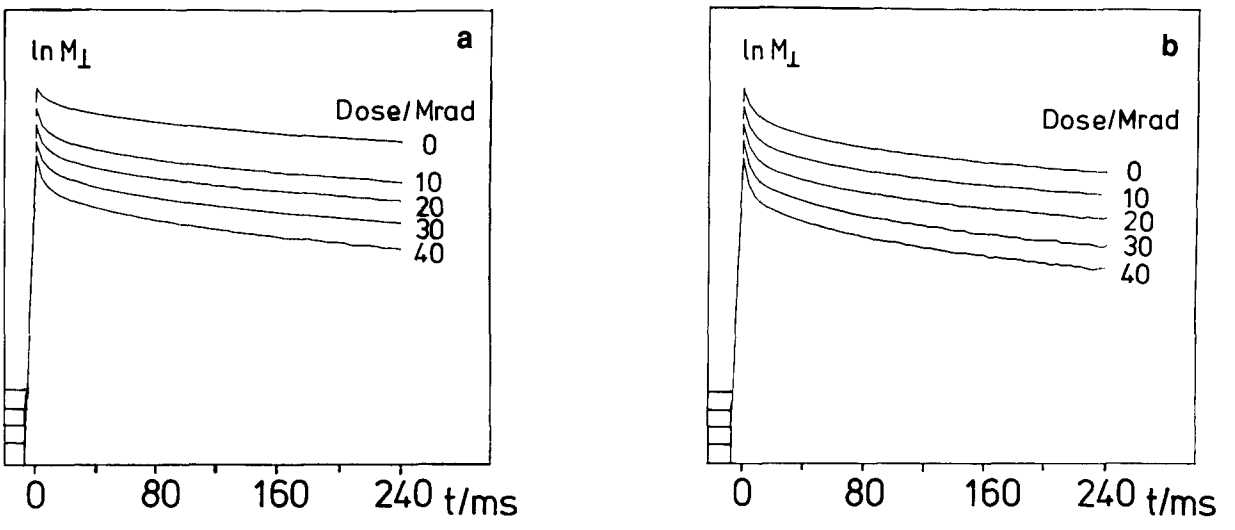

Figure 8 Semilogarithmic plot of the decay of transversal magnetization of $M_\perp$ of (a) HDPE and (b) LDPE in the molten state at 150°C at different irradiation doses. In order to avoid confusion the curves are shifted vertically: the lines at the ordinate indicate the vertical shift of each curve

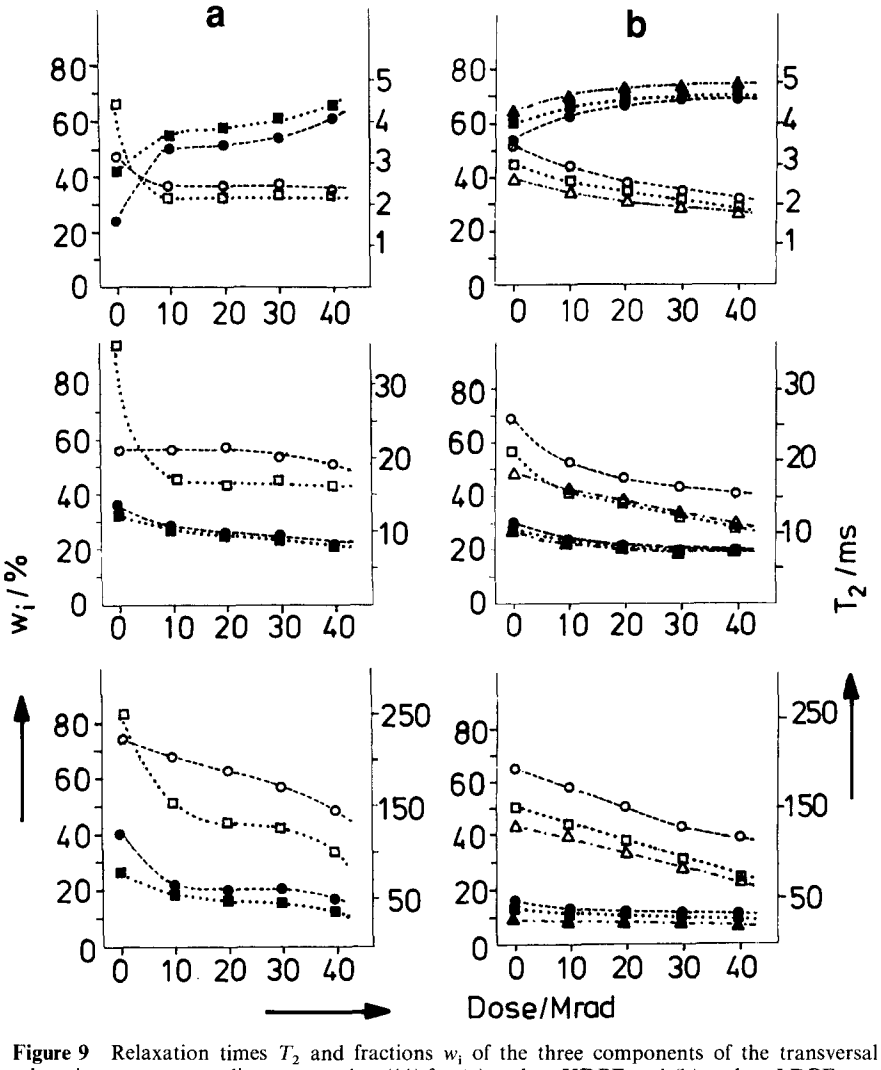

Figure 9 Relaxation times T_2 and fractions w_i of the three components of the transversal relaxation curves according to equation (11) for (a) molten HDPE and (b) molten LDPE as a function of the irradiation dose. The T_2 values are represented by the closed symbols and the w_i values by the open symbols. ●, ○, 150°C; ■, □, 130°C; ▲, △, 110°C

temperature for 24 h. The f.i.d. curves of these recrystallized samples were then measured. The results obtained for HDPE are shown in *Figure 10a*. The f.i.d. curves gradually change with increasing density of crosslinks, the intensity of the rapidly decreasing component becoming smaller. The largest effect is caused by a dosage of only 10 Mrad. The difference between the non-irradiated sample and the sample irradiated at 40 Mrad appears more clearly in the Fourier transform spectrum shown in *Figure 11*. Apparently, the broad component

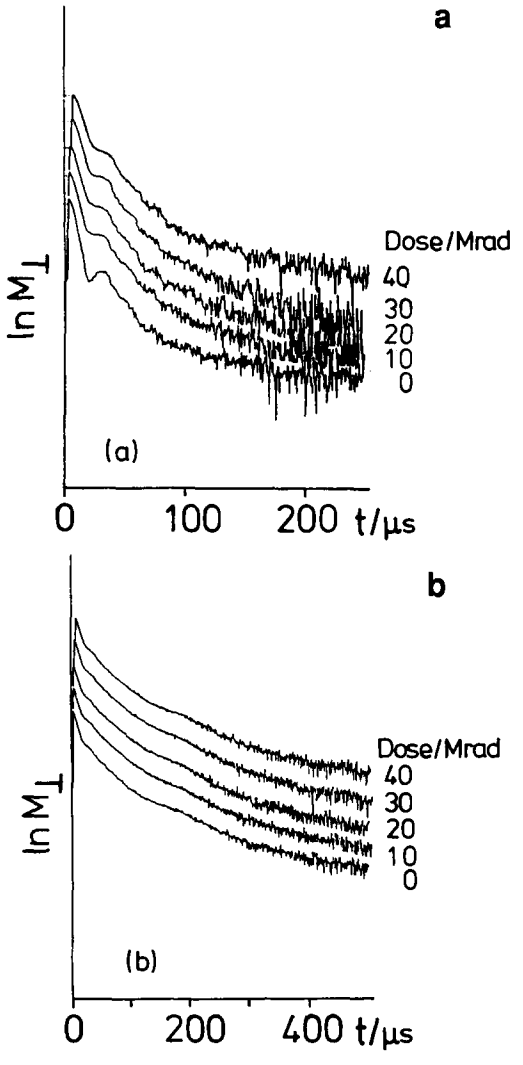

Figure 10 F.i.d. curves of (a) HDPE and (b) LDPE recrystallized after melting for 4 h at 150°C at different irradiation doses

originating from the crystalline part is much smaller in the irradiated sample than in the non-irradiated one. This result indicates that the crosslinks hinder the recrystallization. No such effect was found for LDPE; see *Figure 10b*. If this material is irradiated at doses of up to 40 Mrad, it recrystallizes to the same degree as non-irradiated LDPE.

DISCUSSION

Separation of the f.i.d. curve into different components

Even in the case of a motion which can be explained by a single correlation time τ_c and a single pair τ_{ca} and a describing the anisotropy of motion, according to equations (5) and (6), the f.i.d. curve is not simply a (modulated) exponential curve or a Gaussian curve. Therefore, a separation into different exponential curves according to equation (14), or a separation into a Gaussian curve, an exponential curve and a modulated exponential curve according to equation (13), is not an unambiguous method for the determination of weight fractions w_i and relaxation times T_2^i of chains with different mobility. Without any further consideration, this separation only seems to provide an empirical description of changes in the f.i.d. curve caused by different treatments of the sample.

However, a closer examination of equations (5) and (6) shows that, to a rough approximation, an interpretation of w_i and T_2^i as weight fractions and relaxation times of actually existing chains is correct. Firstly, as stated in the section *Theory. Shape of the f.i.d. curves*, in the case of a single correlation time τ_{ca} and a single anisotropy parameter a, it is never possible to describe the f.i.d. curve by a superposition of several exponential curves because the second derivative of the f.i.d. is always negative. Therefore if a measured f.i.d. curve turns out to be a superposition of several exponential curves, this can be considered as proof that chains really exist that have different T_2 values and/or a values. Secondly, as shown in *Figures 3* and *4*, in the case of a single value of τ_{ca} and a single value of a, the f.i.d. curves can be quite well approximated by a superposition of a Gaussian and an exponential curve which might be modulated in the case of spinning. In the case of high mobility (small values of a and τ_{ca}) a pure exponential curve with a single relaxation time is obtained as shown by the straight lines in *Figures 3* and *4*.

Interpretation of the difference in the crosslink effect between the solid and molten samples

In the solid state of both HDPE and LDPE, no remarkable difference was found between the irradiated and the non-irradiated samples with respect to the ω_r-dependence of the three components of the n.m.r. signal. Only a very small change of the T_2 values of

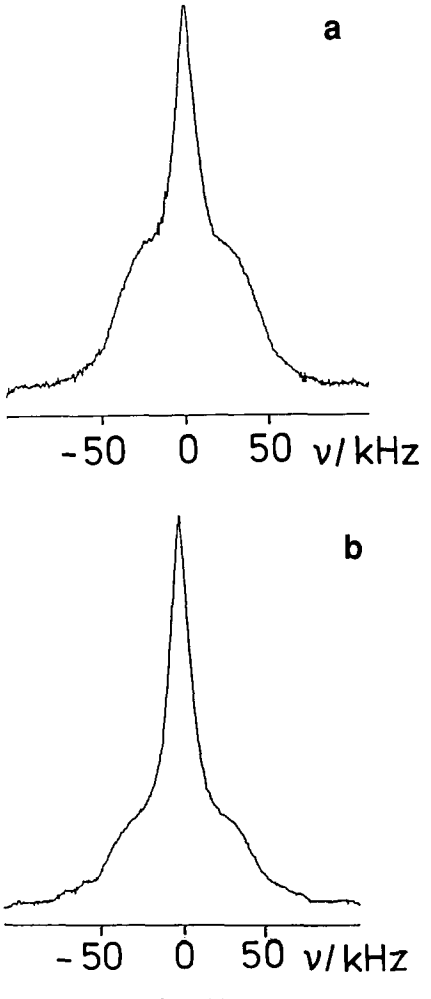

Figure 11 N.m.r. spectrum of HDPE recrystallized after melting for 4 h at 150°C. (a) Non-irradiated; (b) irradiated at 40 Mrad

HDPE was observed upon irradiation (*Figure 7*). On the other hand, a significant crosslink effect was found in the molten state. This could be interpreted as follows. For the non-irradiated HDPE in the solid state, the component 1, which arises from the less mobile part of chains in the amorphous regions, according to its intensity represents approximately 80% of the amorphous chains. Its T_2 value is about 25 μs. This means that the major fraction of the chains in the amorphous regions is quite restricted in mobility. Due to this large fraction of slowly mobile chains, the motion hindering effect of the crosslinks formed by irradiation doses of up to 40 Mrad, is comparatively small. It is thus rather difficult to detect a motion effect of the crosslinks on the chain mobility. However, as reported by Charlesby and Folland[4], in the case of irradiation doses higher than 50 Mrad the crosslinks cause a change of both T_1 and T_2.

In the molten state, the shortest value of T_2 is much larger, i.e. several milliseconds, and the fraction of component 1 is smaller than in the solid state (see *Figure 9*). Therefore the hindering effect of the crosslinks is not masked by the less mobile fraction and crosslinking causes a large decrease in mobility. In addition, an important factor is whether or not the crosslinks are formed at all, rather than the density of crosslinks. This is the reason for the abrupt changes found between 0 Mrad and 10 Mrad in most cases. In other words, n.m.r. measurements in the molten state are more sensitive to crosslinks than measurements on the solid sample. Such a sensitive detection of crosslinks was also reported for e.s.r. measurements on samples in the liquid state[18].

The difference of chain mobility in the melt and in the amorphous regions of the semicrystalline material can be explained by considering the densities of entanglements. In molten polyethylene, the average molecular weight of a chain between two entanglements is 2000 g mol^{-1} according to Porter and Johnson[19] and 8000 g mol^{-1} according to Folland and Charlesby[20]. These values give entanglement densities of 1.5×10^{20} cm^{-3} and 3.8×10^{19} cm^{-3} respectively. These values are of the same order of magnitude as those of the crosslink densities. Therefore, in molten polyethylene crosslinking strongly affects the mobility of the molecules. The situation is completely changed, however, if the polyethylene is crystallized. It is generally assumed and has been shown experimentally, for example for poly(ethylene terephthalate)[21], that during crystallization of polymers the entanglements are expelled from the crystals and are accumulated in the amorphous regions. Therefore, the entanglement density in these regions is much higher than in the melt. As a consequence, the mobility of the chains is smaller than in the melt and crosslinks are of less influence. In addition to the increased density of entanglements, the fixing of the ends of the amorphous chains on the surfaces of the crystals will also decrease the mobility.

Difference in the recrystallization between HDPE and LDPE

It was found that recrystallization after melting was hindered by the crosslinks in the case of the HDPE only, which may be due to the fact that chain branches disturb crystallization. LDPE has many branches, which results in lower crystallinity. Therefore a small density of crosslinks does not affect the crystallization, because crystallization is mainly controlled by the branching. In contrast, the density of branching in HDPE is of the same order or less than the density of the crosslinks formed. These crosslinks therefore hinder the recrystallization.

Determination of the anisotropy parameters a *and* τ_{cb}

Simulation of the f.i.d. curve assuming a single correlation time τ_{ca}. It is well known that a MAS n.m.r. spectrum shows spin side bands under the condition of sufficiently rapid rotation, as illustrated, for example, in *Figure 6b*. The appearance of the side bands corresponds to the modulation of the f.i.d. curve by ω_r, as shown in *Figure 6a*. The modulated f.i.d. curve has been simulated using equation (5) in order to determine τ_{ca}, a and τ_c. The following procedure was used. According to equation (5) the decrease of the intensity of the satellites with increasing time is determined by τ_{ca} while the intensity of the first satellite is proportional to a. The correlation time τ_c is determined from the relaxation time of component 2 in the n.m.r. signal of the rotated sample by means of equation (11). Therefore, to a first approximation, the values of τ_{ca}, a and τ_c were determined by using these relations and a value of M_2 which was obtained from the molecular geometry. These values of τ_{ca}, a and τ_c were then varied until a best fit between the calculated and the measured curves was obtained.

As an example, *Figure 12a* illustrates the best fit simulation of the f.i.d. curve at $\nu_r = 6$ kHz. The parameters used are $\tau_c = 2 \times 10^{-7}$ s, $\tau_{ca} = 3 \times 10^{-4}$ s, $a = 0.23$. A good agreement between the calculated and the measured curve is obtained. However, as shown in *Figures 12b* and *c*, the same set of parameters does not

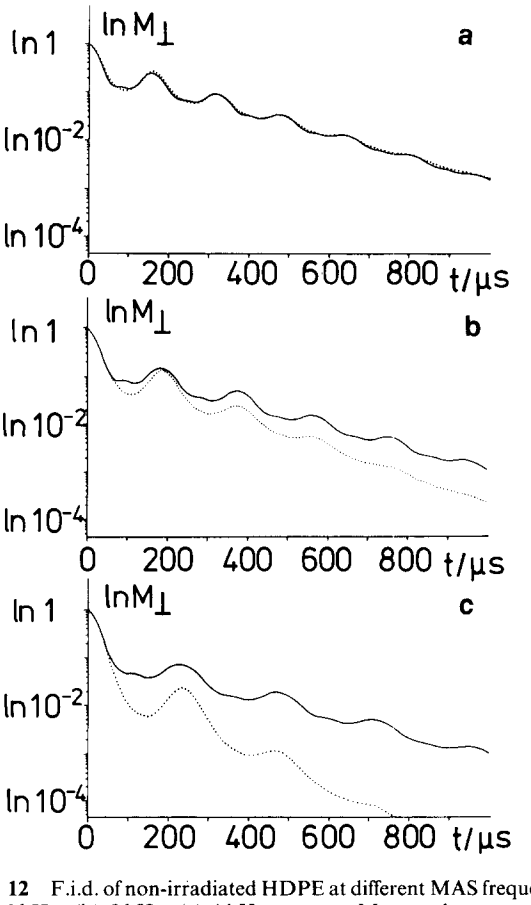

Figure 12 F.i.d. of non-irradiated HDPE at different MAS frequencies ν_r. (a) 6 kHz; (b) 5 kHz; (c) 4 kHz. ———, Measured curves; – – – –, curves calculated assuming $\tau_c = 2 \times 10^{-7}$ s, $\tau_{ca} = 3 \times 10^{-4}$ s, $a = 0.23$

give a good fit for the other values of ν_r such as 5 kHz and 4 kHz. Similar results were obtained for the other samples. It was not possible to fit the f.i.d. curves obtained at different rotation frequencies ω_r with the same set of values of τ_c, τ_{ca} and a for any of the samples. This disagreement indicates that one has to take into account distributions of the correlation times τ_{ca} and/or the anisotropy factors a.

A simple model with a single correlation time τ_{ca} and a single anisotropy parameter a cannot be applied satisfactorily for the following reason. In such a system the n.m.r. line becomes narrower and T_2 becomes larger if the rotation frequency ω_r is larger than a critical value ω_r^*, which is given either by $1/\tau_{ca}$ or by $\sqrt{aM}$, depending on which of the two quantities is larger, i.e.

$$\omega_r^* = \max(1/\tau_{ca}, \sqrt{aM}) \qquad (15)$$

The dependence of T_2 on ω_r is shown schematically in *Figure 13*. The results given in *Figure 7* do not agree with such a behaviour. With increasing ω_r one observes a decrease of the least mobile fraction rather than an increase of T_2 of this fraction. In the following section it is shown that a good fit of the results is obtained if a spectral distribution of τ_{ca} and a is assumed.

Determination of the distribution of τ_{ca} and of a. In the case of a system having a wide distribution of the correlation times τ_{ca} and the anisotropy factors a, the situation is quite complicated. At each rotation frequency, to a first approximation the system has to be divided into two fractions, one satisfying the conditions $\omega_r > \omega_r^*$ and the other satisfying the condition $\omega_r < \omega_r^*$, ω_r^* being given by equation (15). The CH_2 groups satisfying the first condition contribute to the component with the large value of T_2, which is modulated, while the other part of the system contributes to the component having a small value of T_2. With increasing rotation frequency, the number of CH_2 groups contributing to the first component (large value of T_2) increases leading to an increase in intensity of this component of the f.i.d. curve. Thus an apparent phase transition is observed as described by Resing *et al.*[22] for the case of water adsorbed on charcoal, where a broad spectrum of correlation times exists.

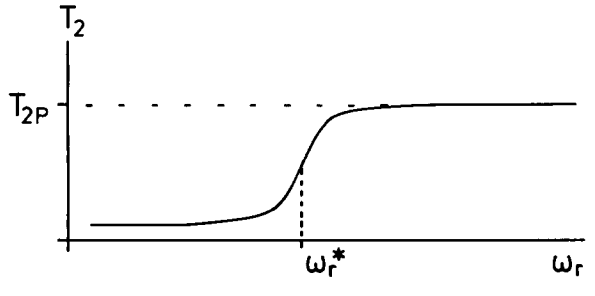

Figure 13 Schematic representation of the dependence of the relaxation time T_2 on rotation frequency ω_r

This situation is illustrated in more detail in *Figure 14*. The spectrum of τ_{ca} and a values of the chains is indicated by the shaded square. The straight horizontal and vertical lines are attributed to different rotation frequencies ω_r. The region above each horizontal line in the diagram is that for $\omega_r \geqslant 1/\tau_{ca}$ while in the region on the left side of each vertical line the condition of $\omega_r \geqslant \sqrt{M_2 a}$ is fulfilled. Therefore, the darker shaded region within the square indicates the fraction of CH_2 groups that satisfy the conditions $\omega_r \geqslant 1/\tau_{ca}$ and $\omega_r \geqslant \sqrt{M_2 a}$ and that contribute to the slowly decaying part of the f.i.d. curve with a large value of T_2. *Figure 14* shows that this fraction increases with increasing ω_r.

For a quantitative determination of the distribution of the parameters a and τ_{ca}, the f.i.d. is simulated after an initial value of τ_c has been determined from the value of $T_2^{(2)}$. However, a trial and error technique for the best choice of these distributions needs a tremendous amount of computer time. Therefore, model f.i.d. curves were calculated for different orders of magnitudes of a, τ_{ca} and ω_r. Examples of such model curves are shown in *Figure 14*. By comparison of the observed f.i.d. curve with the model curves and successively changing the parameters, the regions of possible values of τ_{ca} and a were estimated. Distribution functions for τ_{ca} and a were assumed, and for τ_{ca}, the logarithmic normal distribution function:

$$P(\tau_{ca}) = \exp - [\ln(\tau_{ca}/t_0)/\sigma]^2 \qquad (16)$$

which is characterized by the two parameters t_0 and σ: t_0 represents the value of τ_{ca} at which $P(\tau_{ca})$ is at a maximum while σ is a measure for the width of the distribution. Such a distribution is observed if an

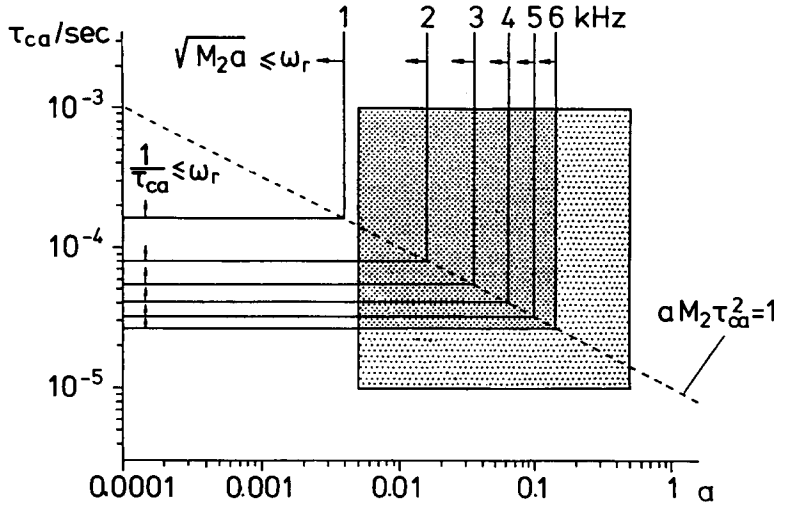

Figure 14 Model for explanation of the measured f.i.d. curves of HDPE and LDPE

Table 2 Correlation time τ_c, parameters t_0 and σ of the distribution of correlation times τ_{ca}, and range of the anisotropy parameter a for the different samples of polyethylene

Sample	τ_c (s)	τ_{ca} (s)			
		t_0	σ	a	$\langle h/h_0 \rangle$
HDPE					
0 Mrad	3×10^{-7}	1×10^{-4}	1.79	0.005–0.50	0.45–0.62
40 Mrad	3×10^{-7}	1×10^{-4}	1.61	0.01–0.65	0.45–0.62
LDPE					
0 Mrad	$3 \times 10^{-7}/5 \times 10^{-8}$	3×10^{-4}	0.85	0.001–0.25	0.22–0.62
40 Mrad	$3 \times 10^{-7}/5 \times 10^{-8}$	3×10^{-4}	0.85	0.001–0.25	0.22–0.62

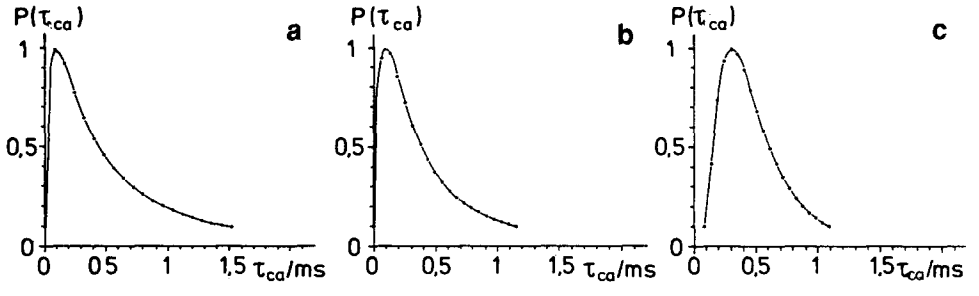

Figure 15 Spectrum of correlation times τ_{ca} assumed for (a) non-irradiated HDPE ($t_0 = 0.1$ ms, $\sigma = 1.78$); (b) HDPE irradiated by 40 Mrad ($t_0 = 0.1$ ms, $\sigma = 1.61$); (c) LDPE irradiated and non-irradiated ($t_0 = 0.3$ ms, $\sigma = 0.85$)

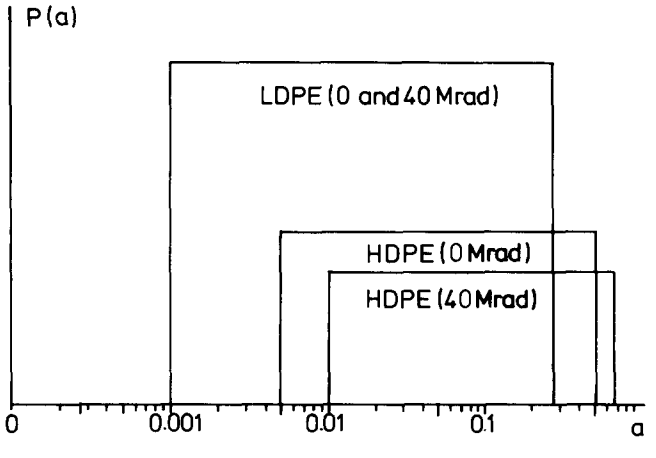

Figure 16 Spectrum of anisotropy parameter for non-irradiated HDPE, for HDPE irradiated by 40 Mrad and for LDPE irradiated and non-irradiated

Arrhenius temperature dependence of τ_{ca} is assumed:

$$\tau_{ca} = \tau_{ca}^0 \exp[E_A/kT] \qquad (17)$$

and a normal distribution for the activation energy E_A. The distribution function for a is assumed to be of a flat box type. By using these distribution functions we simulated the observed f.i.d. and determined the range of a and the parameters t_0 and σ.

of τ_{ca} in the LDPE may be caused by a decrease of the rate of reptation of the chains due to hindrance by side represented in *Figures 15* and *16*. Examples for the comparison between the observed and simulated f.i.d. curves are given in *Figure 17*. The dotted lines represent the calculated curves obtained with the parameters given in *Table 2*. The agreement is satisfactory. In addition, in *Table 2* the average relative end to end distance of the chains between two netpoints formed by entanglements

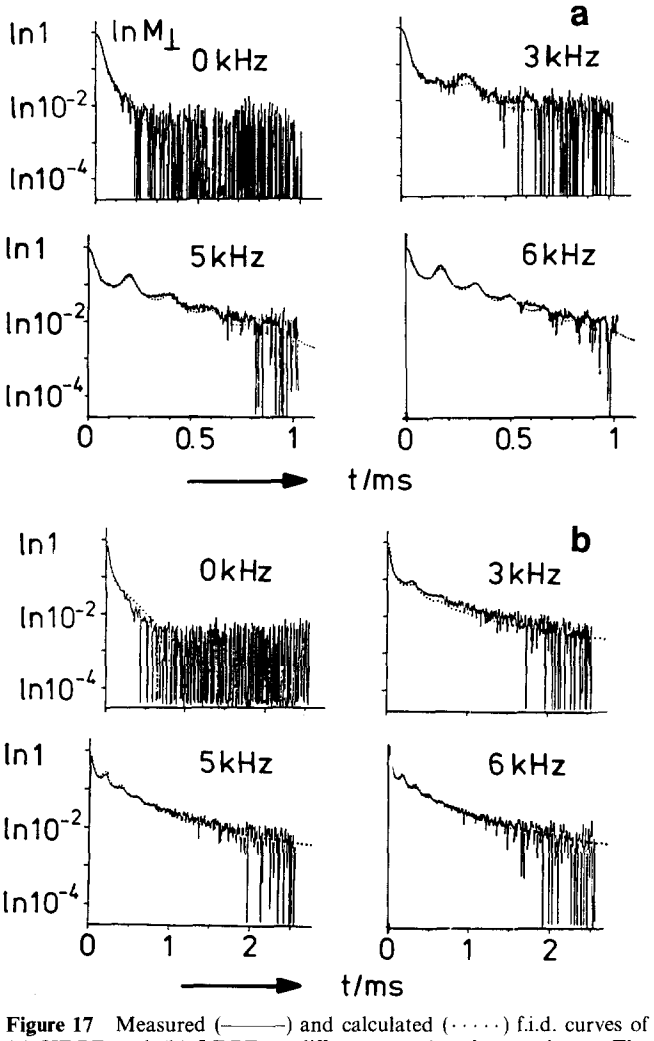

Figure 17 Measured (———) and calculated (· · · · ·) f.i.d. curves of (a) HDPE and (b) LDPE at different rotation frequencies ν_r. The parameters used for the calculation are given in *Table 2*

or crosslinks, $\langle h/h_0 \rangle$ is represented (see *Figure 2*). The values of $\langle h/h_0 \rangle$ were calculated from the contribution of the anisotropy to the reciprocal relaxation time $1/T_{2a}$ given by equation (12). The relation between $\langle h/h_0 \rangle$ and $1/T_{2a}$ has been reported previously[13,14]. The change of h/h_0 reflects some changes in the anisotropy parameter a, though the agreement is not complete. The values of the anisotropy parameter a are thought to be more reliable than those of $\langle h/h_0 \rangle$ because, due to the limitation in the spinning frequency, some error may be involved in the determination of T_{2p} which according to equation (12) is used in the calculation of $\langle h/h_0 \rangle$.

According to *Figure 16*, the anisotropy parameter a for non-irradiated HDPE distributes uniformly from 0.005 to 0.5. This distribution was found to be changed by the crosslinks to another distribution ranging from 0.01 to 0.65. The distribution of τ_{ca} and τ_c are not markedly affected by the crosslinks. Crosslinking has no effect at all in LDPE.

In a very careful evaluation of the result, it is possible to find a fourth component in the f.i.d. curve of LDPE. The appearance of this component can be explained by assuming that about 15% of the CH_2 groups have a smaller correlation time τ_c than the other groups, namely $\tau_c = 5 \times 10^{-8}$ s. These CH_2 groups may be part of short side chains. Alternatively, the fourth component may be explained by assuming that a spectrum of relaxation times τ_c exists in addition to the spectrum in τ_{ca}. This is supported by the fact that the fourth component does not disappear upon spinning under the magic angle.

How can one explain the differences in the spectra of τ_{ca} and a*?*

The values of τ_{ca} are much larger for the LDPE than for the HDPE. τ_{ca}, according to *Figures 1* and *2*, is a measure of the rate of change of the restrictions in motion causing the anisotropy of motion. Therefore the increase of τ_{ca} in the LDPE may be caused by a decrease of the rate of reptation of the chains due to hindrance by side chains. In addition, due to the smaller degree of crystallinity and consequently a smaller accumulation effect during crystallization, the density of the entanglements in LDPE may be less than in HDPE. Thus the time taken for one CH_2 group to move by reptation from one entanglement to the next one (see *Figure 2*) is greater for LDPE than for HDPE.

The effect of crosslinking on τ_{ca} is almost negligible. This indicates that the characteristic lifetime of anisotropy is determined mainly by the entanglements, as a consequence of the comparatively low density of crosslinks. Larger effects may be expected if the irradiation doses exceed 50 Mrad[3,4].

Crosslinking has a significant effect on the distribution of the anisotropy parameter a in HDPE. This effect may be explained by the following consideration. Ideal microbrownian motion is isotropic, in which case the anisotropy parameter $a = 0$. If a hindrance to the microbrownian motion is introduced, i.e. either an entanglement or a crosslink, the molecular motion becomes anisotropic and then $a \neq 0$. The larger the anisotropy the larger the value of a. The results presented in *Figure 16* for HDPE indicate that the chains which have smaller a values are affected by the crosslinks to a larger extent than those with large a values. This could be interpreted as follows. If a crosslink is formed in a region where molecular motion is highly anisotropic before irradiation, the effect on the anisotropy of motion is comparatively small, at least with respect to the analysis performed in this study. If, on the other hand, a crosslink is formed by irradiation in a part in which molecular motion is less anisotropic (region of smallest a values in *Figure 16*) the crosslinks formed produce rather strong hindrance to the molecular motion and the parameter a is shifted from smaller to larger values. The fraction of smaller values of a disappears in this case. This interpretation is consistent with the result of this study, i.e. that the crosslink effect was found to be much stronger in the molten state than in the solid state.

Why does crosslinking not affect the distribution of a in LDPE? It is probable that branches decrease the influence of crosslinks in a way which is not understood at present. This assumption is supported by the results obtained in the melt, where the influence of radiation on mobility is also smaller in LDPE than in HDPE (see *Figure 9*). It is also supported by the result that in LDPE crosslinking has no effect on the amount of recrystallization from the melt, in contrast to the situation in HDPE.

In which regions are the crosslinks formed?

One of the problems relating to the radiation induced crosslinks is whether or not preferential regions for the crosslinks exist. That is, the crosslinks are formed by radiation preferentially in either crystalline regions or amorphous regions or if they are formed without any preference. From the present results it cannot be deduced whether or not crosslinks are formed in the crystals. However it has been proved that crosslinks are formed in the amorphous regions of HDPE because the crosslink effect was found in the n.m.r. signal after the subtraction of the contribution from the crystalline part from the observed signal. In addition, the anisotropy factor a is mostly affected by the crosslinks in the regions of smallest a value, as described in the previous section. The smaller value of the anisotropy factor a is closer to pure isotropic motion, which is only possible in pure amorphous regions. This formation of crosslinks in amorphous regions, as deduced from this research, agrees with the conclusion of an earlier study[15].

ACKNOWLEDGEMENT

One of the authors (J.S.) would like to express his cordial thanks to the Deutsche Forschungs Gemeinschaft for financial support enabling his stay as a visiting professor in the Institute for Technical and Macromolecular Chemistry, University of Hamburg.

REFERENCES

1 Kaike, M., Sohma, J. and Odajima, A. *J. Phys. Soc. Japan* 1957, **12**, 272
2 Ishikawa, K., Kashiwabara, H., Matsuo, H. and Sohma, J. *Rep. Prog. Polym. Phys. Japan* 1966, **9**, 417
3 Folland, R. and Charlesby, A. *Radiat. Phys. Chem.* 1976, **8**, 555
4 Charlesby, A. and Folland, R. *Radiat. Phys. Chem.* 1980, **15**, 393
5 Charlesby, A. and Jaroskiewicz, E. M. *Eur. Polym. J.* 1985, **21**, 55
6 Andrew, E. R. and Jasinski, A. *J. Phys. C* 1971, **4**, 391
7 Schneider, B., Pivcova, H. and Doskocilova, D. *Macromolecules* 1972, **5**, 120
8 Müller, R. and Zachmann, H. G. *Colloid Polym. Sci.* 1978, **64**, 249
9 Müller, R. and Zachmann, H. G. *Colloid Polym. Sci.* 1980, **258**, 753

10 Charlesby, A. 'Atomic Radiation on Polymers', Pergamon, Oxford, 1960
11 Spiess, H. W. in 'NMR Basic Principles and Progress', Vol. 15 (Eds. P. Diehl, E. Fluck and R. Kosfeld), Springer, Berlin, 1978, p. 55
12 Müller, R. Dissertation, University of Hamburg, 1980
13 Scholtyssek, G. Dissertation, University of Hamburg, 1988
14 Schmedding, P. and Zachmann, H. G. *Colloid Polym. Sci.* 1972, **250**, 1105; 1975, **253**, 441; 1975, **253**, 527
15 Rosenke, K. and Zachmann, H. G. *Prog. Colloid Polym. Sci.* 1978, **64**, 245
16 Zachmann, H. G. *J. Polym. Sci., Symp.* 1973, **43**, 111
17 Klüver, W. and Ruland, W. *Prog. Colloid Polym. Sci.* 1978, **64**, 255
18 Murata, K., Shiotami, M. and Sohma, J. *Rep. Prog. Polym. Phys.* 1987, **30**, 591
19 Porter, R. S. and Johnson, J. F. *Chem. Rev.* 1966, **66**, 1
20 Folland, R. and Charlesby, A. *J. Polym. Sci., Polym. Lett. Edn* 1978, **16**, 339
21 Zachmann, H. G. and Günther, B. *Rheol. Acta* 1982, **21**, 427
22 Resing, H. A., Thompson, J. K. and Krebs, J. J. *J. Phys. Chem.* 1964, **68**, 1621
23 Resing, H. A., Thompson, J. K. and Krebs, J. J. *J. Phys. Chem.* 1965, **43**, 669